Static holes in the geometrically frustrated bow-tie ladder



2008 J. Phys.: Condens. Matter 20 415204

(http://iopscience.iop.org/0953-8984/20/41/415204)

IOP PUBLISHING JOURNAL OF PHYSICS: CONDENSED MATTER

J. Phys.: Condens. Matter **20** (2008) 415204 (7pp) doi:10.1088/0953-8984/20/41/415204

# Static holes in the geometrically frustrated bow-tie ladder

**George B Martins**[1] **and Wolfram Brenig**[2]

[1] Department of Physics, Oakland University, Rochester, MI 48309, USA
[2] Institut für Mathematische und Theoretische Physik, TU Braunschweig, 38106 Braunschweig, Germany

E-mail: martins@oakland.edu and w.brenig@tu-bs.de

Received 1 July 2008, in final form 14 August 2008
Published 12 September 2008
Online at stacks.iop.org/JPhysCM/20/415204

**Abstract**

We investigate the doping of a geometrically frustrated spin ladder with static holes by a complementary approach using exact diagonalization and quantum dimers. Results for thermodynamic properties, the singlet density of states, the hole-binding energy and the spin correlations will be presented. For the undoped systems the ground state is non-degenerate, with translationally invariant nearest-neighbor spin correlations. For the doped case, we find that static holes polarize their vicinity through a localization of singlets, reducing the frustration. This polarization induces short range repulsive forces between two holes and an oscillatory behavior of the long range two-hole energy. For most quantities investigated, we find very good agreement between the quantum dimer approach and the results from exact diagonalization.

## 1. Introduction

Geometric frustration is a key factor, leading to exotic phases in quantum spin systems. Valence bond (VB) ordering, with and without breaking of discrete lattice symmetries, is one possible type of ground state symmetry. Examples are the spin-1/2 zig-zag ladder [1], the checkerboard lattice [2, 3], the $j_1$–$j_2$–$j_3$ model [4, 5], or the Shastry–Sutherland model [6]. Another exotic phase is the spin liquid (SL) which displays no apparent magnetic order but may break topological symmetries, which presumably is the case for the two-dimensional (2D) spin-1/2 kagomé antiferromagnet (AFM) [7–9].

Static holes, i.e. nonmagnetic defects, are an important probe of such quantum phases. In case of enhanced VB correlations or VB order without broken lattice symmetries, the situation is similar to spin-ladders and the 2D Heisenberg AFM, where static holes generate spin-1/2 moments in their vicinity [10–12]. The latter induce triplet excitations at low energies. In a SL, e.g. in the kagomé AFM, a very different scenario has been observed, in which singlet pairs accumulate close to the holes, rather than spin-1/2 moments [13]. In case of VB states with spontaneous breaking of the lattice symmetry [14], and other valence bond ground states [15], bound spin-1/2 moments also seem to be absent. Apart from the properties of a single static hole, correlation effects between two holes may shed light on the (de)confinement of mobile carriers, studied by the $t$–$J$ model [20] in frustrated quantum magnets [16–19]—at least for kinetic energies small compared to the exchange coupling, i.e., $t \ll J$. Along this line, hole–hole interactions have been studied recently in the kagomé AFM [13] and in quantum dimer models [21]. In both cases, deconfinement of the static holes has been found. For two recent $\mu$SR-studies of doped kagomé AFMs, see [22, 23].

Additional insight into the response of frustrated spin models to static holes can be obtained from a reduced description of the singlet sector in terms of short range resonating valence bonds [24], so-called quantum dimers (QDs) [25, 9]. Classical dimer models on bipartite lattices allow for a height representation and tend to be confining, with a linearly or logarithmically attractive 'string potential' between holes [26, 27]. Non-bipartite lattices lack a height representation and allow for both, confining as well as deconfining [28–32] phases. Similar behavior is likely for QD models.

In this work we intend to shed further light on the role of static holes in geometrically frustrated magnets by studying the spin-1/2 AFM on a bow-tie ladder (BTL). The BTL is a one-dimensional array of corner sharing triangles, as depicted in figure 1, and may be viewed as the medial lattice of the two-leg ladder [30]. The AFM Heisenberg model on the BTL with nearest-neighbor exchange

$$H = \sum_{\langle lm \rangle} \mathbf{S}_l \cdot \mathbf{S}_m \qquad (1)$$

 

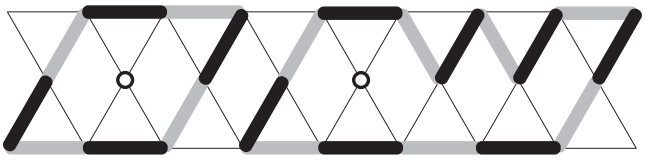

**Figure 1.** 1D bow-tie lattice structure of corner sharing triangles. Spin-1/2 moments reside on all vertices. Thick gray (black) bonds correspond to one QD configuration. Combination of gray and black QDs represent one transition graph. Circles at the center correspond to two static holes.

has been investigated extensively by linear spin wave theory, exact diagonalization (ED) and density matrix renormalization group (DMRG) in [33]. This analysis has uncovered several issues which remain open. In particular, ED on up to $N = 30$ sites suggests that the BTL is qualitatively similar to the Kagomé AFM, i.e. the system is a SL with a spin gap and a large number of singlets ($\propto N^2$) below the first triplet. However, ED does not allow extrapolation of the triplet gap to the thermodynamic limit. DMRG up to $N = 120$ indicates a vanishing spin gap for $N \to \infty$. Therefore, apart from a SL state it remains possible that the BTL is critical or displays VB order with a very large unit cell. Here, we will not focus on these properties of the clean BTL in the thermodynamic limit. Instead, we will investigate the local correlations of *two static holes*—vacancies hereafter—introduced into finite BTLs. The paper is organized as follows. In section 2, a brief description is given of the two numerical methods used. Section 3 compares the specific heat obtained with the ED and QD approaches for the clean system (no vacancies). Section 4 analyzes the change in the density of states caused by the introduction of vacancies; the binding energy of two vacancies; and the spin–spin correlations in the presence of vacancies. Section 5 discusses the results obtained and section 6 presents the conclusions.

## 2. Numerical methods

In this paper, results from two complementary methods will be discussed, namely, complete ED on the one hand, and restricted diagonalization in the QD subspace on the other hand. Recently, QDs on a BTL lattice have been considered for the so-called $\mu$-model of shortest length resonance moves for the QDs. There, for certain ad hoc resonance amplitudes, the QD model was shown to be identical to the transverse-field Ising chain at criticality [30]. In contrast to that study, we will account for all resonance moves resulting from equation (1).

The generalized eigenvalue problem in the QD Hilbert space uses the transition graphs depicted in figure 1 and is set up according to [34] (to which we refer the reader for details). The ED calculations use a Lanczos algorithm [20] when only the ground state properties are needed, and a Householder algorithm when knowledge of the full spectra is necessary. Periodic boundary conditions (PBC) apply to all results discussed in the following and the ED calculations take advantage of all the symmetries available to minimize the size of the Hilbert space. For all systems studied we

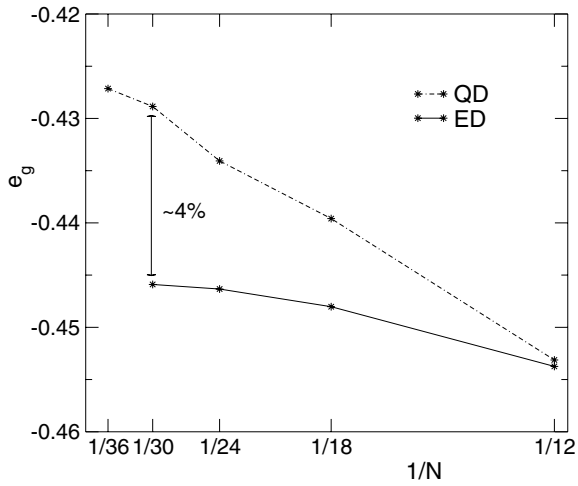


**Figure 2.** Ground state energy versus inverse system size for $N = 12$–$30$ (ED) and $N = 12$–$36$ (QD).

find the undoped ground state to be non-degenerate, with translationally invariant nearest-neighbor spin correlations, which is consistent with a spin liquid state or a valence bond crystal with a unit cell large compared to the system's sizes. Before calculating thermodynamic properties in section 3, the authors wish to compare the ground state energy per spin for different cluster sizes calculated using ED (full Hilbert space) with that calculated using the QD approximation. In figure 2, we show the ground state energy (per spin) $e_g$ versus the inverse system size $1/N$. For QDs, proper $N$ needs to be a multiple of 6 (note that a very small 'even/odd' oscillation with respect to $N/6$ can be seen in the QD results). From figure 2, a deviation of approximately 4–5% between ED and QD can be extrapolated in the thermodynamic limit. This has to be contrasted against the relative dimension $D$ of the complete Hilbert space, $D_0$ of the singlet sector, and $D_{\rm QD}$ of the QD space, which are $D = 2^N$, $D_0 = N!/[(N/2)!(1 + N/2)!]$, and $D_{\rm QD} = 2^{N/3+1}$. For $N = 30$, this implies $D/D_0/D_{\rm QD} \approx 1.1 \times 10^9/(9.7 \times 10^6)/(2.0 \times 10^3)$. In view of these ratios, the results in figure 2 are in reasonable agreement. This seems to indicate that the BTL (with and without vacancies, as stressed in the next sections) has a ground state that can be well described by a wavefunction built exclusively with singlet dimers (which is the essence of the QD approach). A better test of the quality of the singlet dimers ground state wavefunction would be the calculation of its overlap with the ED ground state. These results will be presented elsewhere [35].

## 3. Thermodynamic properties

First, we briefly consider the clean system and compare the specific heat, obtained by ED, with results from the QD approximation. A fingerprint of SL states in strongly frustrated magnets is the accumulation of singlet states at low energies. In the kagomé AFM, the number of singlets below the first triplet has been observed to grow exponentially with system size [8]. In the BTL, power-law behavior with an exponent 2 has been suggested [33]. The singlet accumulation at low

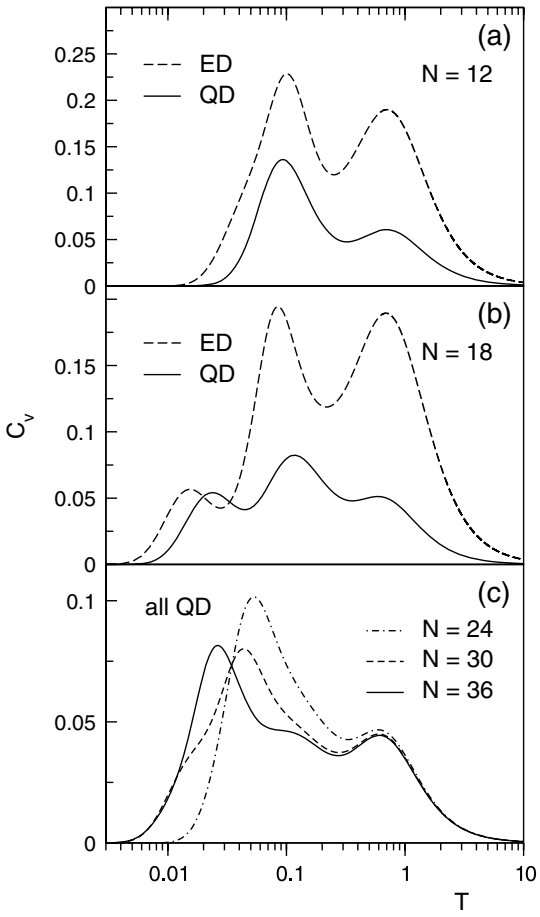


**Figure 3.** Specific heat $C_V$ versus temperature $T$. (a) and (b) Comparison of ED and QD for $N = 12$ and 18. (c) QD for $N = 24$–36.

energies leads to a characteristic singlet–triplet double-peak structure in the specific heat $C_V$ [7, 33, 36, 37]. For the kagomé AFM a substantial fraction of the singlet peak in $C_V$ is believed to be due to QD fluctuations [34]. For the BTL, this is an open issue. Therefore, in figure 3 we consider $C_V$ from QD and ED calculations. The latter agree with identical results from [33]. In view of large finite size effects our emphasis is on a comparison at identical system sizes, rather than in the thermodynamic limit. First, there is a remarkable similarity between the positions of peaks in ED and QD in figures 3(a) and (b). Second, for the leftmost peak in figure 3(b), at low temperatures, the magnitude of $C_V$ and the entropy from ED and QD are comparable. I.e., we conclude that the low-$T$ peak in $C_V$ of the BTL is caused primarily by QD fluctuations. As can be seen from figure 3(c), the low-$T$ peak stabilizes as $N$ increases. Third, in the high-energy region $T > 0.5$ a single peak can be observed which contains most of the entropy (note the log $T$-scale). This entropy is significantly larger in the ED as compared to the QD. This difference is due to triplet excitations not present in the QD space. Figure 3(c) shows that $C_V$ from QD has converged to the thermodynamic limit for $T > 0.1$ at $N > 36$—a system size we cannot reach with ED. Finally, the intermediate-$T$ feature in ED seems strongly system size dependent, as already noted in [33].

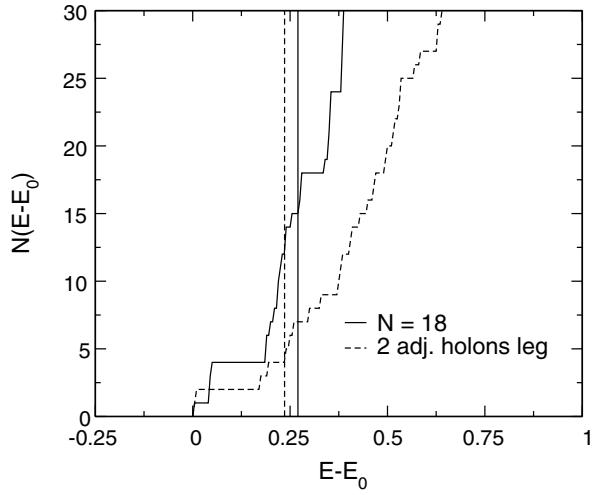


**Figure 4.** Number of singlets in ED versus energy at $N = 18$, contrasting 0 vacancies (solid line) with 2 vacancies (dashed). Solid (dashed) vertical line: triplet gap for 0 (2) vacancies. Vacancies are located at two adjacent sites on one BTL leg. $E_0$ refers to ground state energy.

## 4. Static holes

In this section, we consider the change in the singlet density-of-states (DOS), the binding energy, and the spin correlations which stem from introducing two vacancies into the BTL.

### *4.1. Density of states*

Figure 4 shows the integrated singlet DOS versus energy, contrasting the case of zero vacancies against that of two vacancies placed at adjacent sites on the leg of a BTL with an even number of sites. The main point of this figure is the number of singlets below the first triplet. Evidently this number is reduced by introducing the vacancies. A similar effect is observed for any other relative separation of the vacancies and also in the case of a single vacancy. This low-energy suppression of singlet DOS originates from the reduction of frustration at the neighboring sites of the vacancies, which favors binding of singlets in the vicinity of the vacancies (see also section 4.3). Consequently the low-energy singlet DOS decreases, while the triplet gap is set by excitations distant from the vacancies and therefore less affected. While similar effects have been reported for the kagomé AFM [13], this behavior is drastically different from VB states on bipartite lattices, where static holes tend to bind spin-1/2 moments which leads to an increase of low-energy triplet DOS [38].

While the QD variational space does not contain triplet excitations, it is nevertheless instructive to compare the impact of vacancies on the singlet DOS between the ED and QD calculations. In figure 5, we show the number of singlets above the ground state energy in the QD case for a system size and a vacancy placement identical to that of figure 4. First, the overall trend for QDs depicted is remarkably similar to that in ED. Second, the suppression sets in at somewhat larger energies, of $E - E_0 \sim 0.3$ for QDs, as compared to

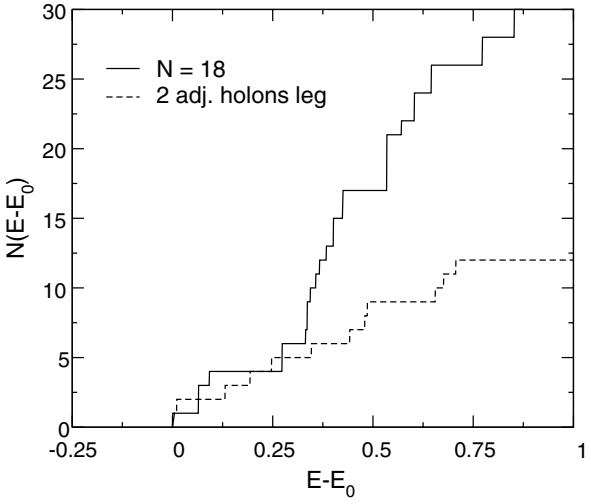


**Figure 5.** Number of QD singlets versus energy at $N = 18$, contrasting 0 vacancies (solid line) with 2 vacancies (dashed). Vacancies are located at sites identical to figure 4. $E_0$ refers to ground state energy.

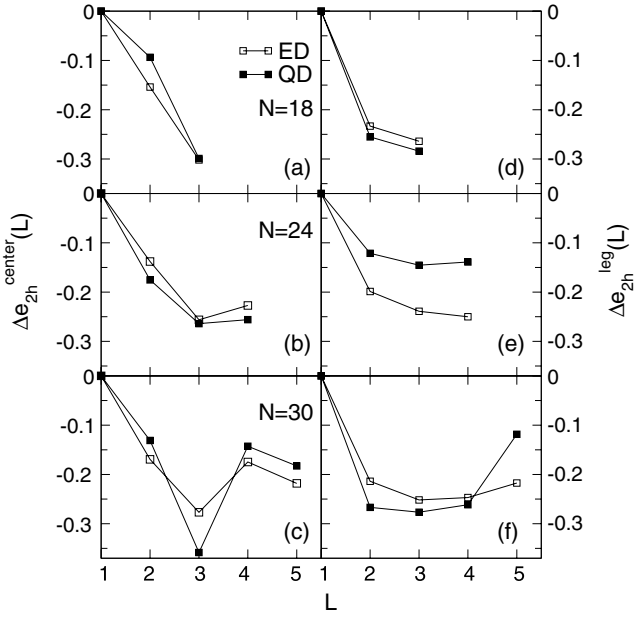


**Figure 6.** Comparing two-vacancy energies at vacancy separation $L$ from ED (solid line with open squares) with QDs (solid line with solid squares) for different systems sizes $N = 18$, 24, and 30. (a)–(c) ((d)–(f)) refer to two vacancies in (on) the center (leg) of the BTL.

$E - E_0 \sim 0.2$ for ED. Finally, it can be seen that in the energy window depicted the QD singlets make up for approximately 50% of the total number of singlets in ED.

As discussed in section 2, the QD basis comprises a small fraction of the singlet sector in the total Hilbert space (used in the ED calculation). It is then expected that the integrated density of states obtained by ED (figure 4) should be considerably larger than that obtained by QD (figure 5). The striking result is that the *change* in the density of states with the introduction of vacancies is similar for ED and QD. This is an indication that the ground state of the BTL is properly described by an SL-like wavefunction composed of singlet dimers (which lies at the heart of the QD approach).

### *4.2. Two-vacancy energy*

Now, we turn to the binding energies

$$\Delta e_{2h}{}^{a}(L) = E_0^a(L) - E_0^a(L = 1) \qquad (2)$$

of two vacancies separated by $L$ sites along the center(leg) $= a$ of the BTL, where $E_0^a$ refers to the corresponding ground state energies. In figures 6 and 7 we present two aspects of $\Delta e_{2h}{}^{a}(L)$. In the former, we compare the binding energies obtained from ED with those from QDs for various systems sizes. First, and remarkably, the ED and QD results are very similar, both for $a$ = center and leg. Second, these figures demonstrate that the vacancies experience a short range repulsive force, with a maximum binding energy at approximately 3 lattice sites. This is in sharp contrast to quantum AFMs with VB ground states on bipartite lattices. There, two vacancies experience a maximum binding energy if placed on those nearest-neighbor sites which are occupied by singlet dimers in the undoped case. Moreover, separating the vacancies will generate a string of 'misplaced' dimers of length proportional to the vacancy separation. This generates a confining potential. Such confinement cannot be inferred

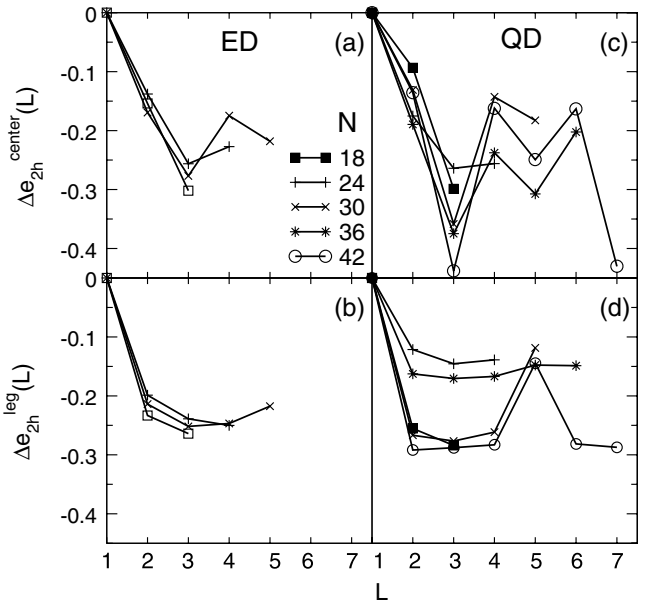


**Figure 7.** Evolution of two-vacancy energies at vacancy separation $L$ with system size for ED with $N = 18$–30 in (a), (b) and for QDs with $N = 18$–42 in (c), (d), with symbols as indicated in panel (a).

from figure 6. Rather, from the largest system which allows for a direct comparison between ED and QDs, i.e. $N = 30$, an oscillatory behavior at large distances can be anticipated. This can be corroborated by extending the QD calculation to larger system sizes as shown in figure 7. There, clear oscillations in $\Delta e_{2h}{}^{a}(L)$ can be observed in the right panel, both on the legs and in the center. In section 4.3, an intuitive picture of

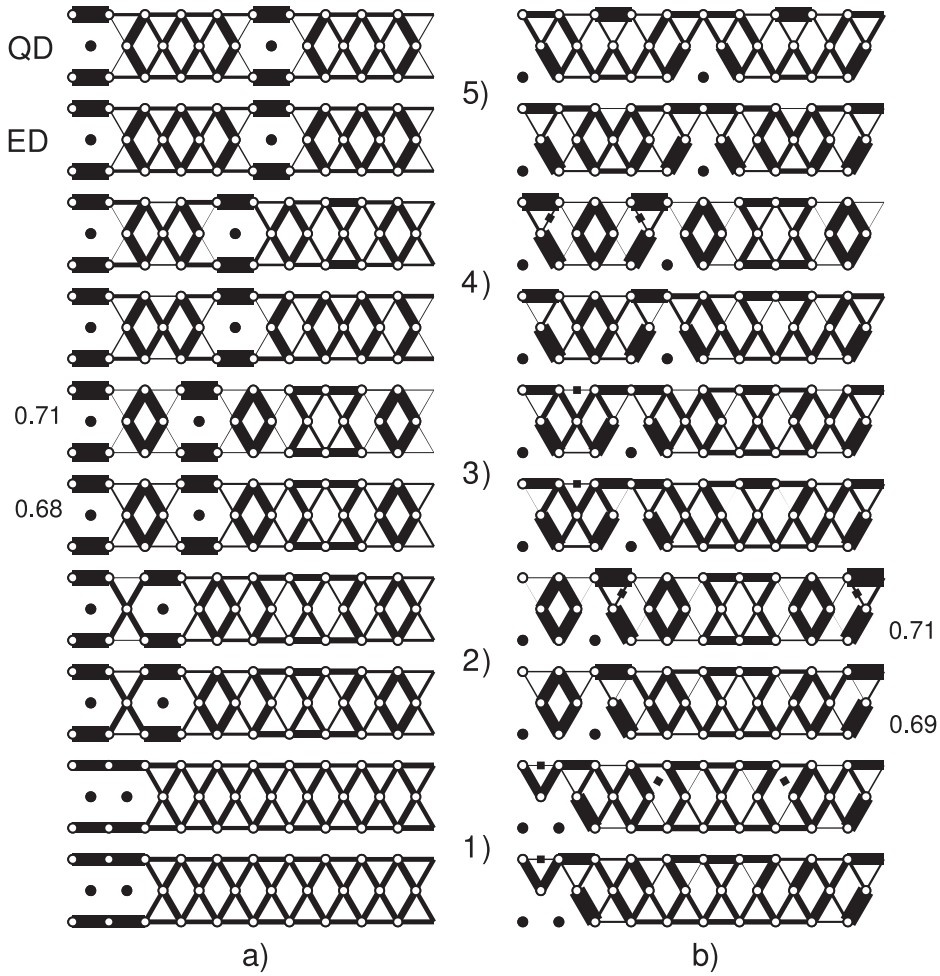


**Figure 8.** Nearest-neighbor spin–spin correlations $s_{lm}$ from ED and QDs, for two vacancies (full circles) on the center and leg of a BTL with $N = 30$ for (a) and (b). The width of solid lines (with vertical slash) is a linear measure of $-s_{lm}$ ($s_{lm}$) for $s_{lm} < 0$ ($>0$). (1) $\cdots$ (5) labels all non-equivalent two-vacancy positions. For each (1) $\cdots$ (5) the adjacent lower (upper) graph corresponds to one ED (QD) result, both for (a) and (b). Numbers refer to maximum values of $-s_{lm}$ observed for ED and QDs in (a) and (b).

the two-vacancy energies in terms of the dimer coverings will arise. From the preceding, it is tempting to speculate that mobile vacancies on the BTL are bound only weakly and will deconfined already for kinetic energies small compared to $J$.

Finally, figure 7 points towards some of the limitations of the QD approach. While the qualitative behavior is identical for ED and QDs, i.e. panels (a) versus (c) and (b) versus (d), panel (d) shows a significant variation of the absolute value of the QD binding energies, depending on whether $N/6$ is even or odd. The latter even/odd effect is absent in the ED results.

### *4.3. Spin–spin correlations*

The nearest-neighbor spin–spin correlations $s_{lm} = \langle \mathbf{S}_l \cdot \mathbf{S}_m \rangle$ are a direct measure of the singlet amplitude on the bond $lm$. Here, we consider the impact of two vacancies on $s_{lm}$ at zero temperature. Figure 8 summarizes our results, both for ED and QDs on the largest system for which we have performed ED, i.e. $N = 30$. In this figure $s_{lm}$ is visualized in terms of 'bond-thickness'. First, we note that $s_{lm}$ fulfils the sum rule

$$E_0(L) = \sum_{lm} s_{lm} \tag{3}$$

where $E_0(L)$ refers to the ground state energy with two vacancies in a relative configuration denoted by $L$. Using the results from figures 6, 7 and 2, the sum rule has been checked to hold for all cases we have studied, both for ED and QDs and also for the undoped case, which will not be discussed here. From figure 8, it is evident that the vacancies introduce a strong polarization into the magnetic background, which leads to spatial oscillations of the spin–spin correlations, with a pattern depending on the separation of the vacancies. This has to be contrasted against the undoped case, in which $s_{lm}$ is almost homogeneous along the BTL with only a very small transverse difference between the central rungs and the legs. Specifically, the figure demonstrates that $s_{lm}$ tends to be largest in the vicinity of the vacancies. This corroborates the picture of a doping induced reduction of singlet fluctuations, due to singlet-binding to the vacancies as discussed in section 3. In fact, the maximal values of $|s_{lm}|$ in the vicinity of the vacancies

as shown in the figure are close to 3/4, implying a singlet amplitude of 1 on those bonds. Note that for a small number of bonds, ferromagnetic correlations of a rather small absolute magnitude arise, both in ED and for QDs.

The tendency of the system to accommodate singlets next to the vacancies provides for a direct interpretation of the vacancy-repulsion, namely the number of 'strong' singlets which can be bound to the vicinity of the vacancies is less if their separation is small. This can be read off directly from figure 8 in going from panel (1) to (5).

For the majority of vacancy placements depicted in figures 8(a) and (b), namely (a) (1)–(3), and (5) as well as (b) (1)–(3), the qualitative real-space structure of $s_{lm}$ is remarkably similar for ED and QDs. For group (a) (4) there are some differences observable right of the second vacancy. In groups (b) (4) and (5) there are clear qualitative differences between ED and QDs, especially on the leg free of vacancies. This suggests that QDs provide for a better description of vacancies in the 'bulk' of the BTL than on its boundaries.

For a quantitative comparison between ED and QDs, we turn to figure 9, where we show several cuts along the BTL through the legs and rungs displaying the values of $-s_{lm}$ versus a measure of distance given by a '1D center-of-mass' CM of each bond. CM runs in steps of 2 (1/2) from 0 ($-1/2$) to $2N/3-2$ ($2N/3-3/2$) on the legs (rungs). The top four panels in figure 9 are representative of those cases in figure 8 which suggest qualitative agreement between ED and QD. It is readily apparent that there is also excellent quantitative agreement. The lower two panels in figure 9 refer to $-s_{lm}$ on the upper leg (rung) for the worst case of figure 8(b) (5), where ED and QD show strong qualitative differences.

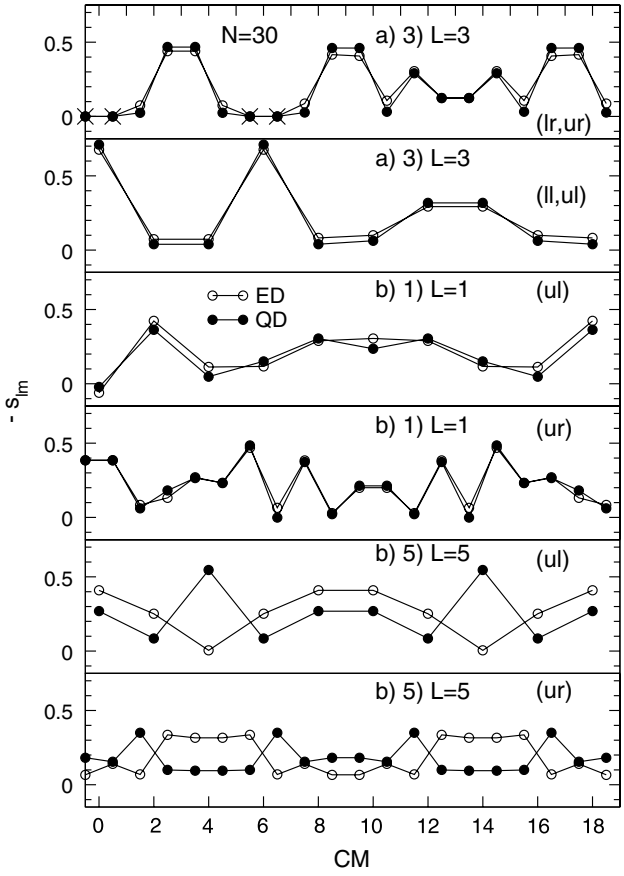


**Figure 9.** Negative nearest-neighbor spin–spin correlations $-s_{lm}$ along the upper (lower) leg (rung) for u(l) l(r) from ED (QDs) for open (closed) circles with two vacancies and $N = 30$, corresponding to figure 8 and panels (a) (3), (b) (1), and (b) (5). CM labels 'center of mass' of bonds. Crosses mark bonds linked to vacancies where $s_{lm}$ has been set to 0.

## 5. Analysis of results

In the following, we provide additional discussion of the results shown in figures 6–9. When both vacancies are positioned in the center axis (see figure 8(a)), reflection symmetry around this axis is retained. This allows for the formation of highly symmetric and simple spin structures. First, as noted above, isolated singlets form at the bonds situated closest to the vacancies for all vacancy separations. Second, more subtle geometrical constraints decide if other spin structures (e.g., loops with even numbers of spins or short chains) will form, where they will be located, and how much singlet correlations there will be between them. For example, in figure 8(a) (3), at a vacancy distance of $L = 3$, apart from the four isolated dimers, one can clearly notice the presence of 4- and 8-spin loops in the shape of three diamonds and a four-pointed star, respectively. These structures are only weakly connected by singlet correlations[3]. Obviously, the distance between the vacancies is one of the controlling parameters in this respect. For example, at distance $L = 5$, open 3-spin chains are present in the shape of boomerangs, besides diamonds and dimers. However, in this case, these structures are not as independent from each other, i.e., the singlet links between them are stronger, as compared to $L = 3$. Therefore, some vacancy distances are more favorable than others in allowing for the formation of such independent 'frustration releasing' structures. This leads to the oscillating behavior of the binding energy in figure 7(c)[4]. Finally, since weakly connected dimers, boomerangs, and diamonds can be described rather well by the QD basis, the very good quantitative agreement between ED and QD for vacancies located in the center axis is no surprise.

When the vacancies are both on the same leg, reflection symmetry around the central axis is lost. Therefore, apart from the dimers close to the vacancies, simple structures as described above are less favorable and form only for some vacancy distances, as for example the diamonds seen at $L = 2$ in figure 8(b). Instead, and in contrast to the centered vacancies, more complex correlations of the spins occur, which involve the presence of 'spin chains' of considerable length. These cannot form when the vacancies are in the center axis because of symmetry considerations and avoidance of

[3] The analysis of figures similar to figure 8 for smaller clusters (not shown) presents the same picture, i.e., at distance $L = 3$ (vacancies in center axis) these simple structures are very well defined and quite weakly connected to each other, resulting in a strong binding energy for vacancies at this particular distance.

[4] It is interesting to note that a criterion that appears to be followed in the formation of these structures is the avoidance of isolated 'free' spins.

uncorrelated free spins. These chain structures with longer range spin–spin correlations are not well described by the QD basis. Their presence leads to quantitative discrepancies with the ED results. The difference in agreement between figures 7(a) and (c) versus figures 7(b) and (d), as well as the discrepancies in the two lower panels in figure 9 corroborate this interpretation[5].

Finally, we would like to repeat that the finite systems we have investigated show a non-degenerate ground state with a triplet gap and many singlet excitations of lower energy. This is suggestive of a spin liquid state and allows for a direct interpretation of the ground state energy oscillations in terms of the RVB picture. For bow-tie ladders in the thermodynamic limit, the generalized Lieb–Schultz–Mattis theorem [39] indicates either a degenerate ground state with a gap to low-energy excitations or a non-degenerate ground state with gapless excitations—favored by DMRG calculations [33]. While we are definitely not able to discriminate between these two cases, it seems very interesting for future studies to clarify if also in the latter case ground state energy oscillations could occur as a function of vacancy separation.

## 6. Conclusions

In summary, we have performed a complementary numerical analysis of a geometrically frustrated quantum spin ladder with and without static holes using exact diagonalization and a truncated basis of quantum dimers. For the undoped system, we have shown that dimers allow for a reasonable approximation of the ground state energy and the low temperature specific heat. In the doped case, we have shown that the system can release frustration through binding of singlets and other extended unfrustrated spin structures to the static holes. Results for the vacancy binding energies and the nearest-neighbor spin correlations confirm this picture. Analysis of dynamic correlation functions, as e.g. magnetic Raman scattering, and the finite size scaling of overlaps between ED and QD states, will be presented elsewhere [35].

## Acknowledgments

Fruitful discussions with E Dagotto and A Albuquerque are gratefully acknowledged. One of us (WB) acknowledges the kind hospitality of the National High Magnetic Field Laboratory at Florida State University in the early stages of this project. Part of this work has been supported by DFG grant No. BR 1084/2-2 and BR 1084/2-3. GBM acknowledges support from Research Corporation (Contract No. CC6542). GBM thanks E Dagotto for the use of a 32 Gigabytes Altus 3400 quad-Opteron workstation located at University of Tennessee in Knoxville.

[5] The presence of these spin-chain structures is easier to spot in spin–spin correlations for smaller clusters than the one shown in figure 8 (with 30 sites). Therefore, the study of varying cluster sizes at constant vacancy doping is needed for a more detailed analysis of the properties of these structures.

## References

[1] Majumdar C K and Ghosh D K 1969 *J. Math. Phys.* **10** 1388
Majumdar C K and Ghosh D K 1969 *J. Math. Phys.* **10** 1399
[2] Brenig W and Honecker A 2002 *Phys. Rev.* B **65** 140407
[3] Fouet J B, Mambrini M, Sindzingre P and Lhuillier C 2003 *Phys. Rev.* B **67** 054411
[4] Singh R R P, Weihong Z, Hamer C J and Oitmaa J 1999 *Phys. Rev.* B **60** 7278
[5] Mambrini M, Läuchli A, Poilblanc D and Mila F 2006 *Phys. Rev.* B **74** 144422
[6] Shastry B S and Sutherland B 1981 *Physica* B+C **108** 1069
[7] Zeng C and Elser V 1990 *Phys. Rev.* B **42** 8436
[8] Waldtmann C, Everts H U, Bernu B, Lhuillier C, Sindzingre P, Lecheminant P and Pierre L 1998 *Eur. Phys. J.* B **2** 501
[9] Misguich G and Lhuillier C 2005 *Frustrated Spin Systems* ed H T Diep (Singapore: World-Scientific)
[10] Martins G B, Dagotto E and Riera J A 1996 *Phys. Rev.* B **54** 16032
[11] Laukamp M, Martins G B, Gazza C, Malvezzi A L, Dagotto E, Hansen P M, López A C and Riera J 1998 *Phys. Rev.* B **57** 10755
[12] Wessel S, Normand B, Sigrist M and Haas S 2001 *Phys. Rev. Lett.* **86** 1086
[13] Dommange S, Mambrini M, Normand B and Mila F 2003 *Phys. Rev.* B **68** 224416
[14] Normand B and Mila F 2002 *Phys. Rev.* B **65** 104411
[15] Kolezhuk A K 1998 *J. Phys.: Condens. Matter* **10** 6795
[16] Read N and Sachdev S 1991 *Phys. Rev. Lett.* **66** 1773
[17] Senthil T, Sachdev S and Fisher M P A 2004 *Science* **303** 1490
[18] Pollmann F and Fulde P 2006 *Europhys. Lett.* **76** 133
[19] Poilblanc D, Läauchli A, Mambrini M and Mila F 2006 *Phys. Rev.* B **73** R100403
[20] Dagotto E 1994 *Rev. Mod. Phys.* **66** 763
[21] Misguich G, Serban D and Pasquier V 2004 *J. Phys.: Condens. Matter* **16** S823
[22] Fukaya A *et al* 2003 *Phys. Rev. Lett.* **91** 207603
[23] Bono D, Mendels P, Collin G, Blanchard N, Bert F, Amato A, Baines C and Hillier A D 2004 *Phys. Rev. Lett.* **93** 187201
[24] Anderson P 1987 *Science* **235** 1196
[25] Rokhsar D and Kivelson S 1988 *Phys. Rev. Lett.* **61** 2376
[26] Fisher M E and Stephenson J 1963 *Phys. Rev.* B **132** 1411
[27] Wu F 2006 *Int. J. Mod. Phys.* B **20** 5357
[28] Misguich G, Serban D and Pasquier V 2002 *Phys. Rev. Lett.* **89** 137202
[29] Fendley P, Moessner R and Sondhi S L 2002 *Phys. Rev.* B **66** 214513
[30] Misguich G, Serban D and Pasquier V 2003 *Phys. Rev.* B **67** 214413
[31] Krauth W and Moessner R 2003 *Phys. Rev.* B **67** 064503
[32] Huse A D, Krauth W, Moessner R and Sondhi S L 2003 *Phys. Rev. Lett.* **91** 167004
[33] Waldtmann C, Kreutzmann H, Schollwck U, Maisinger K and Everts H U 2000 *Phys. Rev.* B **62** 9472
[34] Zeng C and Elser V 1995 *Phys. Rev.* B **51** 8318
[35] Martins G B and Brenig W 2008 in preparation
[36] Elser V 1989 *Phys. Rev. Lett.* **62** 2405
[37] Ramirez A P, Hessen B and Winklemann M 2000 *Phys. Rev. Lett.* **84** 2957
[38] Brenig W 2007 *C. R. Chim.* **10** 79
[39] Cabra D, Honecker A and Pujol P 1988 *Phys. Rev.* B **58** 6241